Global-scale brittle plastic rheology at the cometesimals merging of comet 67P/Churyumov–Gerasimenko

Marco Franceschi[a,b,1], Luca Penasa[c], Matteo Massironi[b,c], Giampiero Naletto[d,c,e], Sabrina Ferrari[c], Michele Fondriest[b], Dennis Bodewits[f], Carsten Güttler[g], Alice Lucchetti[h], Stefano Mottola[i], Maurizio Pajola[h], Imre Toth[j], Jacob Deller[g], Holger Sierks[g], and Cecilia Tubiana[g]

[a]Department of Mathematics and Geosciences, University of Trieste, 34128 Trieste, Italy; [b]Department of Geosciences, University of Padova, 35131 Padova, Italy; [c]Center of Studies and Activities for Space "G. Colombo," University of Padova, 35131 Padova, Italy; [d]Department of Physics and Astronomy "Galileo Galilei," University of Padova, 35131 Padova, Italy; [e]Consiglio Nazionale delle Ricerche - Istituto di Fotonica e Nanotecnologie Padova, 35131 Padova, Italy; [f]Physics Department, Auburn University, Leach Science Center, Auburn, AL 36849; [g]Max Planck Institute for Solar System Research, 37077 Göttingen, Germany; [h]Istituto Nazionale di Astrofisica, Astronomical Observatory of Padova, 35122 Padova, Italy; [i]Institut für Planetenforschung, Deutsches Zentrum für Luft– und Raumfahrt, 12489 Berlin, Germany; and [j]Research Center for Astronomy and Geosciences, Hungarian Academy of Sciences, Konkoly Observatory, 1525 Budapest, Hungary

Observations of comet nuclei indicate that the main constituent is a mix of ice and refractory materials characterized by high porosity (70–75%) and low bulk strength (10^{-4}–10^{-6} MPa); however, the nature and physical properties of these materials remain largely unknown. By combining surface inspection of comet 67P/Churyumov–Gerasimenko and three-dimensional (3D) modeling of the independent concentric sets of layers that make up the structure of its two lobes, we provide clues about the large-scale rheological behavior of the nucleus and the kinematics of the impact that originated it. Large folds in the layered structure indicate that the merging of the two cometesimals involved reciprocal motion with dextral strike–slip kinematics that bent the layers in the contact area without obliterating them. Widespread long cracks and the evidence of relevant mass loss in absence of large density variations within the comet's body testify that large-scale deformation occurred in a brittle-plastic regime and was accommodated through folding and fracturing. Comparison of refined 3D geologic models of the lobes with triaxial ellipsoids that suitably represent the overall layers arrangement reveals characteristics that are consistent with an impact between two roughly ellipsoidal cometesimals that produced large-scale axial compression and transversal elongation. The observed features imply global transfer of impact-related shortening into transversal strain. These elements delineate a model for the global rheology of cometesimals that could be possible evoking a prominent bonding action of ice and, to a minor extent, organics.

comet | impact | deformation | rheology | 67P/Churyumov–Gerasimenko

Imaging of the bilobate comet 67P/Churyumov–Gerasimenko (hereafter 67P) by the Rosetta spacecraft enabled the observation of its surface with unprecedented detail (1). High-resolution images revealed the existence of a pervasive layering, organized into two concentric sets, independently wrapping the two lobes of the comet (2) and whose overall geometric arrangement can be suitably modeled by ellipsoidal envelopes (3, 4). The origin of the layering is unclear, being either primordial or evolutionary (5–7). Although large uncertainty still exists about the nature of comet-forming materials, data from flybys suggest that nuclei are made of high-porosity (70–75%) and low-density (on the order of 10^2 kg m^{-3}) icy and refractory materials (8–12). Very low cohesion of these bodies (tensile strengths of 10^{-6}–10^{-4} MPa) is suggested by the observation of tidal breakup of comets (e.g., D/Shoemaker–Levy 9) (13–15), by studies on tide- and rotation-induced splitting of solid biaxial ellipsoids (16), by results of the Deep Impact experiment (17), and by laboratory experiments and theoretical estimates (18). It should be noted, however, that the presence of discontinuities highly controls bulk strength and hence a high-, or relatively high-strength body, if fractured, can display extremely weak rheological behavior.

Impact modeling has suggested that the bilobate configuration of 67P, which is common to several comet nuclei and Kuiper Belt Objects (e.g., 1P/Halley; 8P/Tuttle; 19P/Borrelly; 103P/Hartley 2; 45P/H–M–P; 486958 Arrokoth), could be due to accretion following multiple, low-velocity (few m s^{-1}) collisions (19, 20). Indeed, given the proposed low bulk strengths, 67P could not have withstood the highly energetic collisions that some models predict as likely in the early stages of cometary evolution (21). Depending on the impact parameters (e.g., angle of incidence, relative speed), impacts would have caused ejection and later reaggregation of material, or transfer and smearing of material belonging to one of the impactors onto the other through flow-like mass-transport mechanisms (19, 22, 23). Nevertheless, no direct evidence of morphologies and structures compatible with

Significance

Unraveling the mechanical behavior of comet-forming materials is key for understanding the genesis and nature of these primordial bodies. We show that the two cometesimals forming comet 67P/Churyumov–Gerasimenko underwent global brittle plastic deformation at the impact that created the bilobate nucleus. Impact-induced deformations were accommodated through large-scale folding of the layered structure and the formation of deep fractures. Axial compression and transversal elongation of the Small Lobe's structure highlighted by three-dimensional modeling indicate that deformation was globally transferred to transversal strain. These features point to a rheological model in which the bonding action of ice with potential contribute of organics is a main factor governing the bulk rheology of cometesimals.

Author contributions: M. Franceschi designed research; M. Franceschi, L.P., M.M., and G.N. performed research; M. Franceschi and L.P. analyzed data; and M. Franceschi, L.P., M.M., G.N., S.F., M. Fondriest, D.B., C.G., A.L., S.M., M.P., I.T., J.D., H.S., and C.T. wrote the paper.

The authors declare no competing interest.

[1]To whom correspondence may be addressed. Email: mfranceschi@units.it.

an impact scenario of bodies made of poorly cohesive materials has been provided yet.

Here we couple three-dimensional (3D) modeling and observations of the surface of 67P to highlight features that tell of global, large-scale brittle-plastic deformation that occurred at the merging of its two lobes and provide direct evidence for the global rheology of the comet.

Three-Dimensional Modeling of 67P

The "onion-like" arrangement of the pervasive layering that characterizes 67P has been demonstrated (2) and it has been shown that the overall geometry of the layered structure is well described by concentric ellipsoidal shells (3, 4) that therefore provide an average approximation of the nucleus layering. Hereafter we will refer to the ellipsoidal models of the lobes as EMs. EMs derive from fitting the terraces (i.e., visible portions of the surfaces of the layers) of each lobe with a family of concentric ellipsoids and provide a model for the layered structure at the lobe scale, but it is important to underline that the shape of the layered structure is not the shape of the lobes (3). The surficial morphology of 67P is the result of the multiplicity of processes (e.g., sublimation, friction produced by reciprocal motion of the lobes, etc.) that have carved the cometary body. The surface of the comet intersects the layered structure, cutting it at variable depth and exposing the layers. In this paper, the term "shape" is used to refer to the shape of the layered structure.

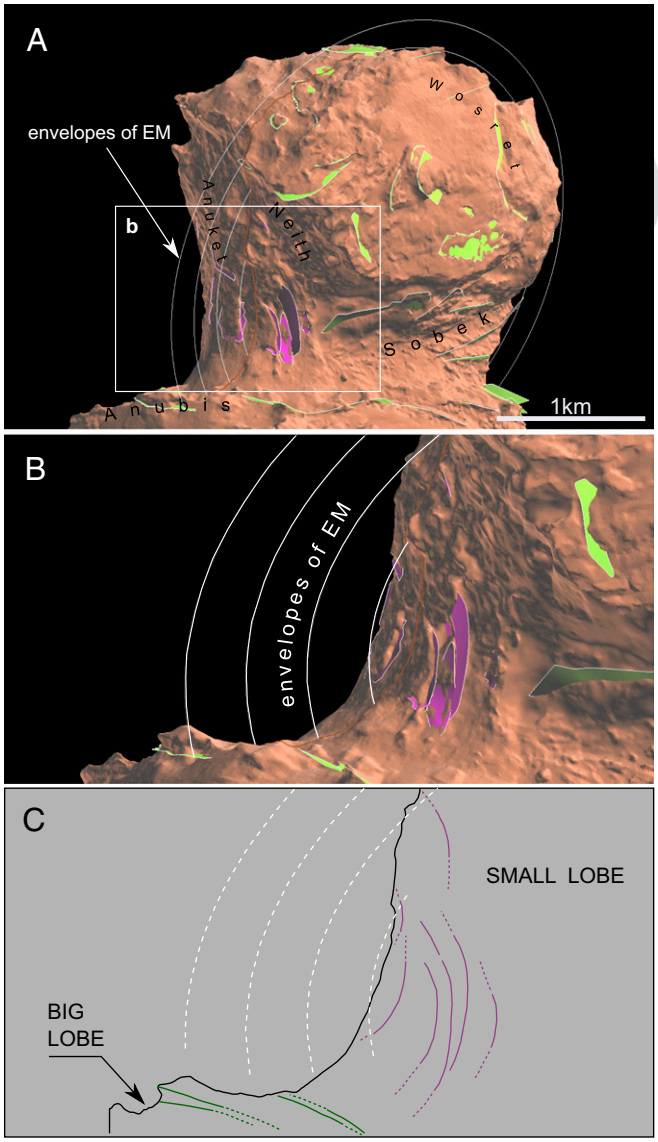

Fig. 1. Evidence of folding of the layering in the neck area of comet 67P. (*A*) View of the Small Lobe and neck area in the shape model (31) of 67P. Some of the layer surfaces used as constraints in the realization of the ILM are shown and those with center of curvature outside the Small Lobe colored in purple. Trend of layering according to the EM is shown as white lines. (*B*) Detail of *A*, showing the opposite concavity between layers of the Small Lobe in the Anuket region and the prediction of the EM. (*C*) Line drawing highlighting features shown in *B*.

Whereas the geometry outlined by the layering of each lobe, in agreement with the EMs, generally has a center of curvature inside the cometesimal, in some regions, and in particular in the Anuket region of the Small Lobe, located in the neck area of the comet, the center of curvature of the layers is instead external with respect to the center of the lobe. In other words, layers locally display a concavity that is opposite with respect to the prediction of the EM. (Fig. 1 *A*–*C*).

To better characterize the geometry of the layered structure and account for the complexity of its shape, we therefore built a geologic 3D model of the comet nucleus, hereafter named Implicit Layering Model (ILM), by applying the SKUA/Gocad modeling suite (24, 25). Both EMs and ILMs are constructed by modeling the layering as a series of contour isosurfaces (i.e., surfaces of equal value) of a 3D scalar field computed on a tetrahedral mesh. However, while the contour surfaces of the scalar field of EMs are assumed to be concentric ellipsoidal surfaces having fixed axial ratios (3), in the ILMs the orientation of the scalar field gradient can be locally varied using constraints to follow the layer orientation and reproduce complex geometries. In our approach, we constrained the local orientation of the gradient of the scalar field to be parallel to the normal of the bedding planes exposed on the surface of the comet. In such a way, we constructed two independent ILMs, one for each lobe (Fig. 2), that are able to represent the local variations in the geometry of the layered structure. Comparison of the EMs and ILMs helps in highlighting how the two models differ.

A convenient way to perform this comparison is considering the average shells of the two models (Fig. 2 *B* and *D*). We define these as the contour isosurfaces corresponding to the average value of the scalar fields of the ILM and EM of the Small Lobe and the Big Lobe and will refer to them hereafter as EM_{AV} and ILM_{AV}. It is worth remarking that ILM_{AV} and EM_{AV} should not be considered as layers *sensu stricto* (i.e., single bedding planes that can be traced in continuity across the entire lobes), but rather as surfaces that represent the organized spatial arrangement of the layers suggested by the orientation of discontinuous terraces distributed on the comet surface.

Differences between the ILM_{AV} and EM_{AV} can be quantified by computing the minimum relative distance between the average shells. This calculation makes it possible to highlight where the layering trend in the ILMs, which more closely follows the actual geometry of the layered structure, substantially offsets from the prediction of EMs and to determine the sign of the offsets. Positive differences between the ILM_{AV} and EM_{AV} characterize areas where ILM_{AV} is in an external position with respect to the EM_{AV} and negative differences characterize areas where ILM_{AV} is internal with respect to EM_{AV}.

Discussion

Large-Scale Deformation of Comet 67P as Suggested by 3D Modeling. Two areas in which the ILM_{AV} is internal with respect to EM_{AV} characterize the Small Lobe (Fig. 3 *A*–*C*): one faces the neck region and the Big Lobe; the other is located approximately to the antipodes of the Small Lobe. Furthermore, a belt along which the ILM_{AV} protrudes with respect to the EM_{AV} surrounds the lobe. The plane (SLP: Small Lobe Plane) that best fits the

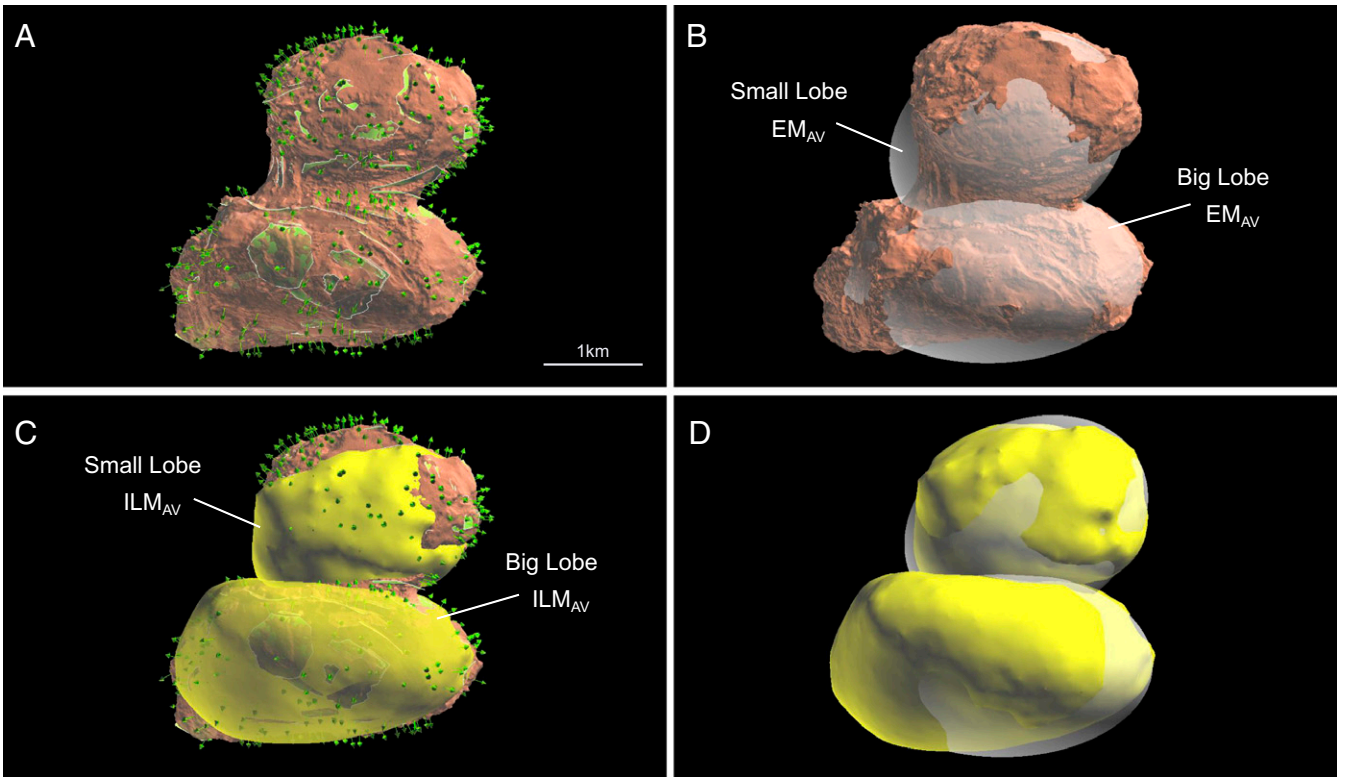

Fig. 2. Three-dimensional ILM of comet 67P realized in Gocad/SKUA (27). (*A*) Constraints used in the implicit 3D modeling procedure. The orientation of the 3D scalar field representing the layering is locally controlled by the constraints. Bedding surfaces and arrows indicating the normal to bedding planes are visible. (*B*) Average shells of the EM (EM_{AV}) of Small Lobe and Big Lobe (3). (*C*) Average shells of the ILM (ILM_{AV}) of Small Lobe and Big Lobe. (*D*) ILM_{AV} (yellow) and EM_{AV} (white) average shells visualized together. The EM_{AV} is shown in transparency to highlight that its shape in places substantially differs with respect to the ILM_{AV}.

maxima of this belt of positive offset of the ILM_{AV} with respect to the EM_{AV} approximately divides the Small Lobe in two equal parts (Fig. 3 *B* and *C*).

The location and sign of the Small Lobe's ILM_{AV} vs. EM_{AV} discrepancies appear not randomly distributed. The two antipodal areas of negative difference are located where compression would be expected if the Small Lobe had crudely ellipsoidal layered structure at the impact with the Big Lobe. Similarly, the belt of positive difference surrounding the Small Lobe ILM_{AV} is located where expansion associated with the aforementioned compression should have developed. The observed features are therefore consistent with the effects of an axial shortening associated with a transversal elongation in a plastic deformation regime undergone by a body with ellipsoidal structure at the impact with the Big Lobe. Furthermore, the observation of the positive-difference ridge on the Small Lobe ILM_{AV} reveals that it lies onto the SLP in the northern hemisphere of the lobe (Fig. 3*B*), while it is asymmetrically folded in the southern hemisphere, where it faces the Big Lobe (Fig. 3*C*). This feature is consistent with deformation associated to dextral strike–slip motion that folded part of the expansion rim after the impact. Remarkably, the asymmetric folding of the positive difference ridge is in kinematic agreement with the structure observed in the Anuket region because the way the layers are bent and the change in their concavity testify deformation with dextral strike–slip kinematics produced by reciprocal motion of the two lobes (Fig. 4).

The Big Lobe's ILM_{AV} also displays areas characterized by positive and negative differences from its EM_{AV}. Although their spatial distribution is not as regular as seen for the Small Lobe, a sector characterized by negative difference between Big Lobe's ILM_{AV} and EM_{AV} faces the neck region. Also this configuration agrees with the deformation of a Big Lobe with elongated ellipsoidlike layered structure at the junction with the Small Lobe (Fig. 5*A*). A positive-difference ridge surrounds this area and interestingly the plane that best fits its maxima (BLP: Big Lobe Plane) is closer to the impact zone than the SLP analogously constructed for the Small Lobe (Fig. 5 *B* and *C*). This is consistent with a depression produced by a more localized deformation that did not involve the entire Big Lobe when it impacted with the smaller Small Lobe. In addition, the SLP and BLP are nearly parallel, but make a small angle that is acute in the direction of bending of the expansion rim on the Small Lobe ILM_{AV}. This feature is also in agreement with the reciprocal motion of the lobes that originated a deformation with a dextral strike–slip kinematics.

Table 1. Parameters used in the realization of the comet 67P ILMs

Number of tetrahedrons of Small Lobe ILM	~2,000,000
Average length of tetrahedron edge of Small Lobe ILM	~150 m
Number of tetrahedrons of Big Lobe ILM	~2,000,000
Average length of tetrahedron edge of Big Lobe ILM	~150 m
Constant gradient constraint	1
Fitting factor	2
Mxdsi iter	−1
Mxdsi error	1e-007
Relative weight constraint on base controller object	1
Relative weight constraint on top controller object	0.001
Relative weight constraint on input layer surface normals	1

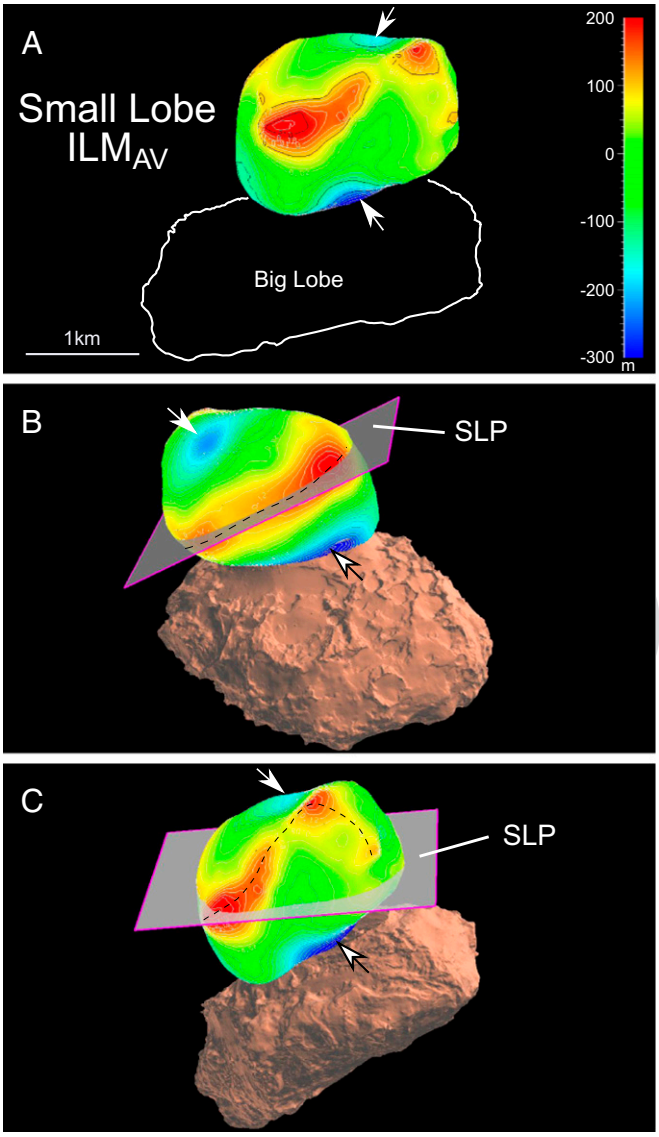

Fig. 3. Comparison between the ILM$_{AV}$ and the EM$_{AV}$ models of the Small Lobe. ILM$_{AV}$ is colored in function of its distance from EM$_{AV}$. Negative differences (blue) correspond to areas where the ILM$_{AV}$ is located in internal position with respect to EM$_{AV}$. Positive differences (red) correspond to areas where the ILM$_{AV}$ is external with respect to the EM$_{AV}$. Arrows mark the areas with negative differences (blue color) located in antipodal position on the Small Lobe ILM$_{AV}$ that are compatible with compression that occurred at the impact between two lobes having roughly ellipsoidal layered structure. (*A*) Small Lobe's ILM$_{AV}$ shell with differences from EM$_{AV}$ shell. (*B*) View of the northern hemisphere of the Small Lobe ILM$_{AV}$ shell. SLP is a plane that best fits the maxima of the positive-differences ridge surrounding the ILM$_{AV}$. The ridge (black dashed line) on the northern hemisphere lays on SLP. (*C*) View of the southern hemisphere. Here, the ridge (black dashed line) does not lay on SLP and is asymmetrically folded.

In summary, the nonrandom distribution of discrepancies between ILMs and EMs is consistent with the plastic deformation that two bodies having an approximately ellipsoidal layered structure would have undergone upon impacting and therefore implicitly suggests the preimpact geometric arrangement of the layering. Although the exact geometry of the layered structure prior to the merger is unknown, an interior structure made of broadly ellipsoidal envelopes acquired in primeval times has been proposed in evolutionary models of the layering (i.e., dual-mode, propagating, phase-change mechanism of Ref. 7). Furthermore, the existence of two independent ellipsoid-like structures is also in agreement with the evidence that the orientation of the layer surfaces is orthogonal to the gravity field of each lobe, indicating that the aggregation/accretion process of the cometary material could have given origin to a structure characterized by radial symmetry (2). Finally, remote observations have shown that a large fraction of cometary nuclei have ellipsoid-like shapes (26, 27) or that, in cases of bilobate nuclei, each of the lobes can be modeled as an ellipsoid (28). Thus, it is reasonable to consider the preimpact structure of the lobes as nearly ellipsoidal.

It is worth mentioning that past events of separation and reimpact of bilobate comets have been also hypothesized as induced by an increase in the spin rate due to sublimation torques that could lead to splitting of the lobes and the generation of gravitationally bounded fragments that would ultimately undergo a low-speed merger (29). Although deformation features observed on 67P are consistent with a single collisional event which resulted in the current bilobate configuration of the nucleus, multiple reconfigurations cannot be excluded, because evidence of such events may have been lost during last impact as a consequence of detachments and nucleus resurfacing. Our analysis may nevertheless provide constraints for exploring multiple separation/reimpact scenarios by means of numerical modeling.

Insights on the Global Rheology of Comet 67P. Layers' heads are widely visible on 67P, especially in the neck area (3). Furthermore, layers clearly penetrate the cometary surface, testifying that the layered structure extends in depth and that bedding has been exposed by erosion and loss of material. Sublimation, the primary phenomenon driving mass loss of the comet, has been estimated to be responsible of a total mass loss of 10.5×10^9 kg, corresponding to ~0.02 km^3 volume of material, during the perihelion passage observed by Rosetta (30). The two ILMs can be used to obtain an approximate independent estimate of the volume of cometary material that is missing with respect to the hypothetic postmerger shape of two intact lobes. The envelopes used for the volume estimate are defined by the contour surfaces that pass through the points of the two lobes' surfaces that occupy the most external position in the scalar fields of the ILMs. According to the ILMs, the volumes of the intact lobes are about 34 km^3 for the Big Lobe and 15 km^3 for the Small Lobe. The present volumes, referring to the shape model of Preusker et al. (31), are about 12.5 and 6 km^3, respectively, implying that ~60% of the volume of the two lobes could be missing. Although being roughly estimated, the loss of such volumes only via sublimation rates would require over 1,500 perihelion passages at present rates. According to studies on the past dynamical history of 67P (32), the comet was orbiting farther than 2 astronimical units prior to 1959 and hence surface activity was nearly absent; therefore, an alternative explanation for the mass loss is required.

The comet surface is characterized by the presence of pervasive fracturing at all scales. This fracturing univocally indicates brittle behavior. Because it is difficult to reconcile this observational evidence with the estimated low strength of the cometary material, the existence of a hardened layer at the comet surface has been proposed (33). Nevertheless, many fractures are several hundred meters long and cut in the layered structure, reaching its deepest parts (Fig. 6). Such fractures cannot be interpreted as thermal contraction cracks, which have actually been observed on 67P, but give rise to a characteristic polygonal fracture network and interest only the surface (34, 35). Furthermore, the occurrence of long fractures is not limited to the neck region (36), where it could be also attributed to the torque forces related to the spinning of the nucleus (29), but it is widespread, suggesting an origin related to an event that globally affected the comet. All these elements indicate that when the two lobes

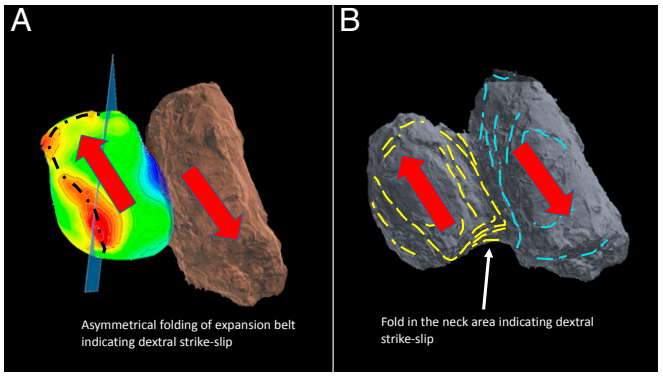

Fig. 4. Features indicative of the reciprocal motion of the two lobes of 67P with dextral strike–slip kinematics (red arrows) that occurred at their merger. (*A*) Asymmetrical folding of the expansion ridge (dotted line) of the Small Lobe ILM_{AV} (see Fig. 3). (*B*) Folding of the layered structure in the neck area (Anuket region of the Small Lobe, Fig. 1). Color scale of ILM_{AV} as in Fig. 3.

merged, in addition to the plastic deformation testified by the layers geometry in Anuket and confirmed by 3D modeling, large-scale brittle fractures formed that were not limited to the surface, but reached deep into the lobes. These fractures can explain the large volumes of missing cometary material as their formation made large detachment possible. Detachments may have occurred either at the time of the impact or later on, favored by mechanisms like the shear movements between the lobes (37), by activity phenomena whose effects may have stimulated/enhanced the fracturing, or by tidal forces during passages close to massive planetary bodies (13–15).

Given the nearly ellipsoidal preimpact structure of the lobes suggested by 3D modeling, the axial compression of the Small Lobe induced by the impact and highlighted by the ILM_{AV}–EM_{AV} comparison can be estimated in about 500 m, ~25% of the diameter of the entire lobe. Given the proposed low strength/high porosity of the cometary material, kinetic energy of the lobes would have been enough, even in case of a low-velocity collision, to induce strong compaction. Hence, high densification associated with such a relevant shortening would be expected, especially in the region of impact. Instead, gravity analyses and radar imaging have shown that 67P gravity field is consistent with a homogeneous body (38, 39). Although this evidence does not exclude the possibility of small-scale differences in density in the comet, it rules out the presence of large density variations within the nucleus. This element points to a global deformation that occurred at nearly constant volume, permitted by the development of pervasive fracturing.

If we define, for the Small Lobe, ΔL_{axial} as the axial shortening and ΔL_{trans} as the transversal elongation, obtained by averaging the maxima of the belt of positive difference between ILM_{AV} and EM_{AV} (Fig. 3 *A*–*C*), we can calculate the ratio $\lambda = \frac{-\Delta L_{trans}}{\Delta L_{axial}}$, obtaining $\lambda = 0.26 \pm 0.05$. The comet being plastically deformed, this ratio closely resembles an effective Poisson's ratio, defined as $\nu = \frac{-\Delta L_{trans}/L_{trans}}{\Delta L_{axial}/L_{axial}}$, where L_{trans} and L_{axial} are the transversal and axial lengths before deformation, respectively. Since the values L_{trans} and L_{axial} are rather similar for the Small Lobe EM_{AV}, it can be said that in this case $\lambda \sim \nu$. A positive λ implies the ability of the cometary material to transfer at global scale the impact-related strain. Deformation features indeed show that the mainly compressive strain at the merging event was transferred in directions perpendicular to the maximum shortening. Moreover, in highly porous granular materials $\nu \to 0$ and therefore the stress generated by the impact should have been accommodated primarily through compaction (40, 41) for which, as mentioned, there is no evidence (38). The results from the 3D model analysis are therefore, also in this case, in agreement with independent observations.

In order to explain the global rheology of 67P, in which the lateral transfer of impact strain in a highly porous granular material and large-scale brittle plastic behavior occurred, we propose a fundamental role played by the binding action of icy volatiles. Depending on the structural mixing, ice can exert a strong influence on the mechanical properties of granular materials, in particular when it is able to form bonds in between grains either through condensation in pore space or later sintering and creeping. Although laboratory experiments have shown that it is hard to produce long-lasting bonds through sintering, this process has been proposed as the one responsible for the formation of a hardened layer on the surface of 67P (42, 43) where the highest compressive strengths were measured (44).

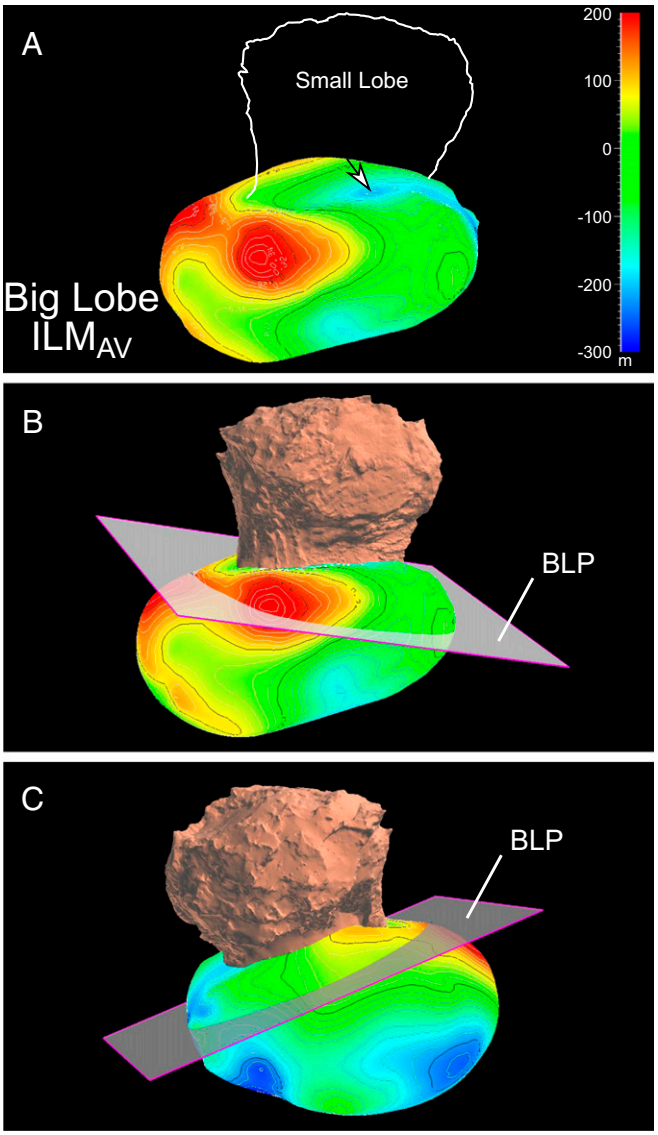

Fig. 5. Comparison between the Big Lobe ILM_{AV} and EM_{AV} models. ILM_{AV} of the Big Lobe is colored as a function of its distance from the EM_{AV}. Color bar as in Fig. 3. (*A*) Big Lobe's ILM_{AV} with differences from EM_{AV} shell. Arrow marks the area with negative difference between Big Lobe ILM_{AV} and EM_{AV} facing the Small Lobe. (*B* and *C*) BLP is the plane that best fits the maxima of the positive-difference ridge around the area with negative difference on ILM_{AV} shell of the Big Lobe (marked by arrow in *A*).

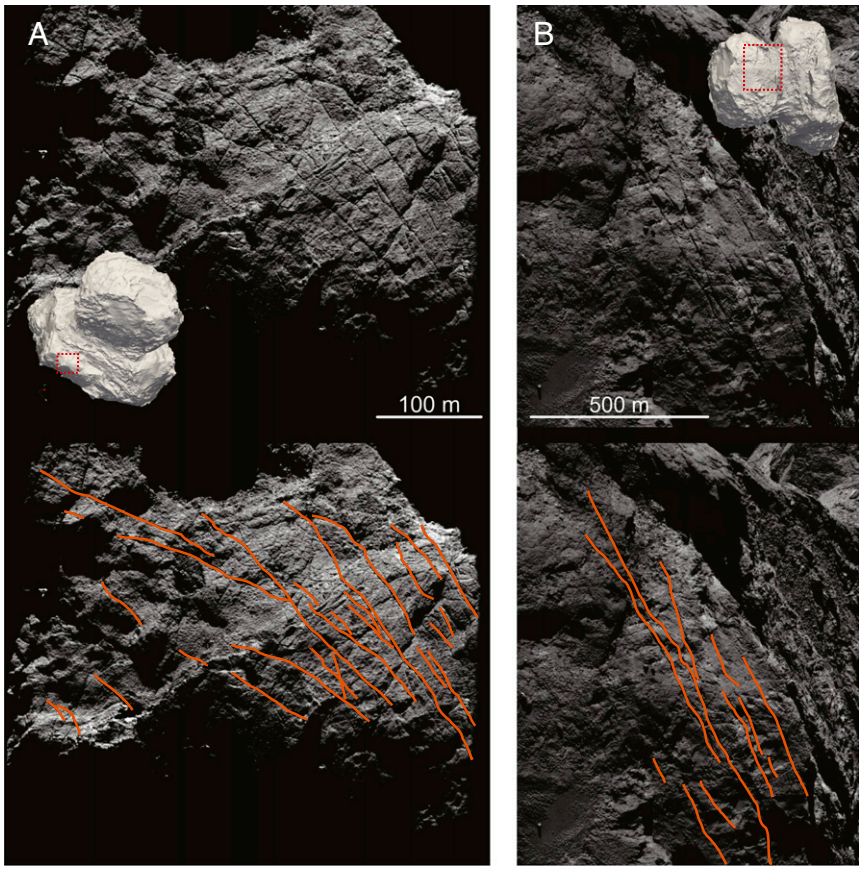

Fig. 6. Large-scale fractures on comet 67P. OSIRIS Narrow Angle Camera images (52) displaying areas of 67P characterized by long, pervasive fractures. The length of the main fractures (orange lines), on the order of several tens of meters, implies that their origin cannot be referred to thermal contraction, but is instead due to large-scale rupture likely linked to the impact between the two lobes. (*A*) NAC_2014–09–30T08.54.41. (*B*) NAC_2016–02–10T07.07.02.532Z_ID30_1397549004_F28 (detail). Location of the areas represented in the images is marked by red dotted squares on the views of the comet shape model (31).

However, it was also shown that, although ice is present on 67P (45, 46), it may represent as little as 16% of its mass (47). Hence, it could be argued that in such low proportions the effect of ice in influencing global-scale rheology could be negligible. Nevertheless, experiments on the mechanical properties of lunar regolith at various degrees of ice saturation (48, 49) and at temperatures of ~77 K have shown that 0.3% in mass of water ice in a regolith with porosity of about 50% (way below saturation) is sufficient to result in compressive strengths on the order of 10 Mpa. It is therefore fair to say that even low amounts of ice could strongly influence the global rheology of 67P, providing the significant stiffness that is indicated by the multiple impact-related global deformation features displayed by its structure.

Another, and potentially concurring, mechanism is the binding capability of organics. Collisional experiments have shown that organics can stick more efficiently and faster than granular ice within the Solar Nebula and these bonds are potentially able to significantly influence the mechanical properties of granular aggregates (50). Hence, also organics may play a role in determining the global rheology of 67P. However, sticking of organics is a process thought to have occurred early in the region of the protoplanetary disk where 67P cometesimals nucleated (50), while icy volatiles condensed later on, providing the possibility of creating intergranular bonds. Furthermore, the refractory dust covering the entire nucleus is essentially cohesionless and is mostly constituted by organics (50). Hence, it is likely that organics contribute little with respect to icy volatiles to the bulk nucleus stiffness.

In conclusion, large-scale structural features indicate that comet 67P underwent global brittle-plastic deformation when the two cometesimals that constitute the nucleus merged, leading to the acquisition of the bilobate configuration. Furthermore, impact-related strain was transferred through the entire layered structure. Such strain transfer indicates significant bulk stiffness of the lobes that we propose provided by the binding action of icy volatiles and, to a lesser extent, organics. Multiple lines of evidence therefore point to a brittle plastic rheology for cometesimals at the comet nuclei–forming impacts.

Materials and Methods

The ILM of comet 67P/Churyumov–Gerasimenko was realized using the Structural Lab plugin of the SKUA/Gocad geomodeling suite (24, 25). The reader is referred to Caumon et al. (24) and references therein for a detailed explanation of the theory behind the implicit modeling algorithm implemented in SKUA/Gocad. Here we recall that the implicit modeling approach, known also as level-set method, considers geological interfaces as isosurfaces or surfaces of equal value of a 3D scalar field, which is computed on a predefined volumetric tetrahedral mesh. The mesh density controls the model resolution. The input data for the realization of the ILMs of comet 67P were terrace surfaces (i.e., layer surfaces) reconstructed by interpolating polylines and point sets derived directly from the comet shape model of the comet (31). Point sets were selected where terrace surfaces were visible; polylines were instead digitized following the bedding. The surfaces were built in SKUA/Gocad by applying the interpolation tools implemented in the software that rely on the Discrete Smooth Interpolator (51). In the implicit modeling approach implemented in the SKUA/Gocad Structural Lab plugin the normal to the layer surfaces at a point is used to reconstruct a scalar field, the gradient of which is parallel to the normals at each input point.

Two independent implicit models were built for the two lobes of comet 67P. In the models, isosurfaces (i.e., layers) never cross or intersect (conformable layering). Moreover, no faults that may displace the layered sequence are considered in the model. We are aware that this is a simplification; however, we believe this approach is reasonable, since our primary goal is to model the global layer arrangement. Furthermore, in order to avoid operator-driven choices in the realization of the model, we did not provide the interpolator with any predefined correlation between the terraces surfaces used as input data.

The Structural Lab Plugin (24) makes it possible to change the degree of fit of the scalar field isosurfaces to the constraint data by setting values of convergence parameters, a roughness constraint, and relative weights to each constraint. All set parameters for the realization of the lobes' ILMs are reported in Table 1. The Structural Lab plugin requires that at least two controller objects are provided as base and top of the modeled series of isosurfaces. We chose as base controller objects (i.e., origins of the scalar fields) the centers of the ellipsoidal models (3) and as top controller objects two ellipsoidal shells extracted from the same model and having major axes with a length approximately twice with respect to the lobes' radii.

ACKNOWLEDGMENTS. This paper is part of a project supported by the European Union's Horizon 2020 Research and Innovation Program under Grant Agreement 776276 (PLANMAP). The Department of Geosciences of the University of Padova provided funding support to this research. The Optical, Spectroscopic, and Infrared Remote Imaging System (OSIRIS) was built by a consortium of the Max–Planck–Institut für Sonnensystemforschung, in Göttingen, Germany, Centro di Ateneo di Studi e Attività Spaziali "Giuseppe Colombo"–University of Padova, Italy, the Laboratoire d'Astrophysique de Marseille, France, the Instituto de Astrofisica de Andalucia, Consejo Superior de Investigaciones Científicas, Granada, Spain, the Research and Scientific Support Department of the European Space Agency, Noordwijk, The Netherlands, the Instituto Nacional de Tecnica Aeroespacial, Madrid, Spain, the Universidad Politechnica de Madrid, Spain, the Department of Physics and Astronomy of Uppsala University, Sweden, and the Institut für Datentechnik und Kommunikationsnetze der Technischen Universität Braunschweig, Germany. The support of the national funding agencies of Germany (Deutsches Zentrum für Luft- und Raumfahrt), Italy (Agenzia Spaziale Italiana), France (Centre National d'Études Spatiales), Spain (Ministerio de Educación y Ciencia), Sweden (Swedish National Space Board), and the Technical Directorate of the European Space Agency is gratefully acknowledged. We thank the European Space Agency teams at European Space Astronomy Centre, European Space Operations Centre and European Space Research and Technology Centre for their work in support of the Rosetta mission. The comments of two anonymous Reviewers have greatly improved the quality of this manuscript.

1. H. Sierks *et al*.,On the nucleus structure and activity of comet 67P/Churyumov-Gerasimenko.*Science* **347**, 1–6 (2015).
2. M. Massironi *et al*., Two independent and primitive envelopes of the bilobate nucleus of comet 67P. *Nature* **526**, 402–405 (2015).
3. L. Penasa *et al*., A three-dimensional modelling of the layered structure of comet 67P/Churyumov-Gerasimenko. *Mon. Not. R Astron. Soc.* **469**, S741–S754 (2017).
4. B. K. Ruzicka *et al*., Analysis of layering-related linear features on comet 67P/Churyumov–Gerasimenko. *Mon. Not. R. Astron. Soc.* **482**, 5007–5011 (2019).
5. B. J. R. Davidsson *et al*., The primordial nucleus of comet 67P/Churyumov-Gerasimenko. *Astron. Astrophys.* **592**, A63 (2016).
6. M. J. S. Belton *et al*., The internal structure of Jupiter family cometary nuclei from Deep Impact observations: The "talps" or "layered pile" model. *Icarus* **191** (supp. 2), 573–585 (2007).
7. M. J. S. Belton, X. D. Zou, J. Y. Li, E. Asphaug, On the origin of internal layers in comet nuclei. *Icarus* **314**, 364–375 (2018).
8. B. J. R. Davidsson, P. J. Gutiérrez, Estimating the nucleus density of Comet 19P/Borrelly. *Icarus* **168**, 392–408 (2004).
9. B. J. R. Davidsson, P. J. Gutiérrez, H. Rickman, Nucleus properties of Comet 9P/Tempel 1 estimated from non-gravitational force modeling. *Icarus* **191** (suppl. 2), 547–561 (2007).
10. M. F. A'Hearn, Comets as building blocks. *Annu. Rev. Astron. Astrophys.* **49**, 281–299 (2011).
11. P. C. Thomas *et al*., Shape, density, and geology of the nucleus of Comet 103P/Hartley 2. *Icarus* **222**, 550–558 (2013).
12. L. Jorda *et al*., The global shape, density and rotation of Comet 67P/Churyumov-Gerasimenko from preperihelion Rosetta/OSIRIS observations. *Icarus* **277**, 257–278 (2016).
13. J. C. Solem, Density and size of comet Shoemaker-Levy 9 deduced from a tidal breakup model. *Nature* **370**, 349–351 (1994).
14. E. Asphaug, W. Benz, Density of comet Shoemaker-Levy 9 deduced by modelling breakup of the parent "rubble pile.". *Nature* **370**, 120–124 (1994).
15. E. Asphaug, W. Benz, Size, density, and structure of comet Shoemaker–Levy 9 inferred from the physics of tidal breakup. *Icarus* **121**, 225–248 (1996).
16. B. J. R. Davidsson, Tidal splitting and rotational breakup of solid biaxial ellipsoids. *Icarus* **149**, 375–383 (2001).
17. M. F. A'Hearn *et al*., Deep impact: Excavating comet Tempel 1. *Science* **310**, 258–264 (2005).
18. Y. V. Skorov, Estimating the strength of the nucleus material of comet 67P Churyumov–Gerasimenko. *Sol. Syst. Res.* **50**, 225–234 (2016).
19. M. Jutzi, E. Asphaug, The shape and structure of cometary nuclei as a result of low-velocity accretion. *Science* **348**, 1355–1358 (2015).
20. D. de Niem, E. Kührt, S. Hviid, B. Davidsson, Low velocity collisions of porous planetesimals in the early solar system. *Icarus* **301**, 196–218 (2018).
21. A. Morbidelli, H. Rickman, Comets as collisional fragments of a primordial planetesimal disk. *Astron. Astrophys.* **43**, 1–9 (2015).
22. M. Jutzi, W. Benz, Formation of bi-lobed shapes by sub-catastrophic collisions: A late origin of comet 67P/C-G's structure. *Astron. Astrophys.* **62**, 1–10 (2016).
23. M. Jutzi, W. Benz, A. Toliou, A. Morbidelli, R. Brasser, How primordial is the structure of comet 67P/C-G? Combined collisional and dynamical models suggest a late formation. *Astron. Astrophys.*, 10.1051/0004-6361/201628963 (2017).
24. G. Caumon, G. Gray, C. Antoine, M. O. Titeux, Three-dimensional implicit stratigraphic model building from remote sensing data on tetrahedral meshes: Theory and application to a regional model of la Popa Basin, NE Mexico. *IEEE Trans. Geosci. Remote Sens.* **51**, 1613–1621 (2013).
25. Emerson, Gocad/SKUA webpage. https://www.pdgm.com/products/skua-gocad/skua-modeling-platform/. Accessed 16 August 2019.
26. P. L. Lamy, I. Toth, Y. R. Fernández, H. A. Weaver, The sizes, shapes, albedos, and colors of cometary nuclei in *Comets II* (Wiley Periodicals, Hoboken, NJ, 2004), pp. 223–264.
27. R. Kokotanekova *et al*., Rotation of cometary nuclei: New light curves and an update of the ensemble properties of Jupiter-family comets. *Mon. Not. R. Astron. Soc.* **471**, 2974–3007 (2017).
28. P. Lamy *et al*., Comet 8P/Tuttle : A portrait of a contact-binary nucleus from hubble and spitzer space telescopes observations. *Geophys. Res. Abstr.* **14**, 10506 (2012).
29. M. Hirabayashi *et al*., Fission and reconfiguration of bilobate comets as revealed by 67P/Churyumov-Gerasimenko. *Nature* **534**, 352–355 (2016).
30. M. Pätzold *et al*., The Nucleus of comet 67P/Churyumov-Gerasimenko–Part I: The global view–Nucleus mass, mass-loss, porosity, and implications. *Mon. Not. R. Astron. Soc.* **483**, 2337–2346 (2019).
31. F. Preusker *et al*., The global meter-level shape model of comet 67P / Churyumov-Gerasimenko. *Astron. Astrophys.* **1**, 1–5 (2017).
32. J. B. Vincent *et al*., Large heterogeneities in comet 67P as revealed by active pits from sinkhole collapse. *Nature* **523**, 63–66 (2015).
33. O. Groussin *et al*., The thermal, mechanical, structural, and dielectric properties of cometary nuclei after Rosetta. *Space Sci. Rev.*, 10.1007/s11214-019-0594-x (2019).
34. M. R. El-Maarry *et al*., Regional surface morphology of comet 67P from rosetta/OSIRIS images : The Southern Hemisphere. *Astron. Astrophys.* **593**, A110 (2016).
35. A. T. Auger *et al*., Meter-scale thermal contraction crack polygons on the nucleus of comet 67P/Churyumov-Gerasimenko. *Icarus* **301**, 173–188 (2018).
36. M. R. El-Maarry *et al*., Fractures on comet 67P/Churyumov-Gerasimenko observed by Rosetta/OSIRIS. *Geophys. Res. Lett.* **42**, 5170–5178 (2015).
37. C. Matonti *et al*., Bilobate comet morphology and internal structure controlled by shear deformation. *Nat. Geosci.* **12**, 157–162 (2019).
38. M. Pätzold *et al*., A homogeneous nucleus for comet 67P/Churyumov-Gerasimenko from its gravity field. *Nature* **530**, 63–65 (2016).
39. V. Ciarletti *et al*., CONSERT suggests a change in local properties of 67P/Churyumov-Gerasimenko's nucleus at depth. *Astron. Astrophys.* **583**, A40 (2015).
40. G. N. Greaves, A. L. Greer, R. S. Lakes, T. Rouxel, Poisson's ratio and modern materials. *Nat. Mater.* **10**, 823–837 (2011).
41. J. M. Greenberg, H. Mizutani, T. Yamamoto, A new derivation of the tensile strength of cometary nuclei: Application to comet Shoemaker-Levy 9. *Astron. Astrophys.* **295**, 36–38 (1995).
42. B. Gundlach *et al*., The tensile strength of ice and dust aggregates and its dependence on particle properties. *Mon. Not. R. Astron. Soc.* **479**, 1273–1277 (2018).
43. B. Gundlach, J. Ratte, J. Blum, J. Oesert, S. N. Gorb, Sintering and sublimation of micrometre-sized water-ice particles: The formation of surface crusts on icy Solar System bodies. *Mon. Not. R. Astron. Soc.* **479**, 5272–5287 (2018).
44. T. Spohn *et al*., Thermal and mechanical properties of the near-surface layers of comet 67P/Churyumov-Gerasimenko. *Science* **349**, 1–5 (2015).
45. A. Rotundi *et al*., Dust measurements in the coma of comet 67P/Churyumov-Gerasimenko inbound to the sun. *Science* **347**, 1–7 (2015).
46. M. Fulle *et al*., The dust-to-ices ratio in comets and Kuiper belt objects. *Mon. Not. R. Astron. Soc.* **469**, S45–S49 (2017).
47. M. Fulle *et al*., The refractory-to-ice mass ratio in comets. *Mon. Not. R. Astron. Soc.* **482**, 3326–3340 (2019).
48. L. Gertsch, R. Gustafson, R. Gertsch, Effect of water ice content on excavatability of lunar regolith. *AIP Conf. Proc.* **813**, 1093–1100 (2006).
49. L. S. Gertsch, J. Rostami, R. Gustafson, "Review of lunar regolith properties for design of low power lunar excavators" in *6th International Conference on Case Histories in Geotechnical Engineering* (Missouri University of Science and Technology, Arlington, VA, 2008), pp 1–16.
50. A. Kouchi, T. Kudo, H. Nakano, M. Arakawa, N. Watanabe, Rapid growth of asteroids owing to very sticky interstellar organic grains. *Astrophys. J.* **566**, L121–L–124 (2002).
51. J. L. Mallet, Discrete modeling for natural objects. *Math. Geol.* **29**, 199–219 (1997).
52. European Space Agency, Rosetta. https://www.cosmos.esa.int/web/psa/rosetta. Accessed 16 August 2019.